Monte Carlo modeling for the computation of in-field and out-of-field doses in 3D conformal radiotherapy of breast cancer

N. Rafat-Motavalli[1,2], H. Miri-Hakimabad[1,2*], E. Hoseinian-Azghadi[1], L. Rafat-Motavalli[1], M. Dayyani[2,3], T. Tuğrul[4]

[1]Department of Physics, Faculty of Science, Ferdowsi University of Mashhad, Mashhad, Iran
[2]Research and Education Department, Reza Radiotherapy and Oncology Center, Mashhad, Iran
[3]Radiation Oncology Department, Reza Radiotherapy and Oncology Center, Mashhad, Iran
[4]Department of Radiation Oncology, Medicine Faculty of Van Yüzüncü Yıl University, Van, Turkey

► ***Original article***

***Corresponding author:**
Hashem Miri-Hakimabad, Ph.D.,
***E-mail:** mirihakim@um.ac.ir*

Received: February 2025
Final revised: October 2025
Accepted: February 2026

Int. J. Radiat. Res., July 2026; 24(3): 763-770

DOI: 10.61186/ijrr.24.3.25

Keywords: *Monte Carlo, breast cancer, radiotherapy.*

ABSTRACT

Background: To generate the Monte Carlo (MC) 3D dose distribution in both in-field and out-of-field regions for three-dimensional conformal radiotherapy (3DCRT) of breast cancer patients and to compare it with the dose calculations from two available commercial treatment planning systems (TPS). ***Material and Methods:*** The Prowess Panther TPS was initially used to create the treatment plan and underwent a simulation process using the MCNPX 2.6.0 Monte Carlo code. Dose maps, profiles, dose volume histograms (DVHs), and mean doses for organs at risk (OARs) were calculated. To evaluate the accuracy of dose calculations, global gamma index analysis was conducted to ensure conformity between MC dose calculations and the two TPSs. ***Results:*** For individual beams, comparing Prowess to MC shows that the gamma passing rates (GPR) range from 94.3% to 99.2%, with a GPR of 91.2% for all beams combined. In contrast, when comparing RayStation to MC, the GPRs range from 96.0% to 99.0%, with a total beam GPR of 94.3%. Regarding out-of-field doses, the two TPSs can provide reliable dose calculations only for organs receiving mean doses greater than 500-700 cGy. ***Conclusion:*** The MC model was benchmarked for 3DCRT plans, demonstrating that it could provide accurate MC doses in the in-field area. Furthermore, the comparison between MC and TPS doses shows that RayStation performs better in the in-field region. Nonetheless, both TPS-based out-of-field estimates were unreliable, indicating the importance of utilizing MC methods to estimate out-of-field doses.

INTRODUCTION

The rising incidence of breast cancer (BC) presents a significant public health challenge globally [1]. An estimated 2.3 million women were diagnosed with BC in 2020, with an overall recurrence rate of 30%; it accounts for 6.6% of deaths among women worldwide [2]. In light of this serious situation, it is vital to focus on BC diagnosis and treatment options [3]. Treatment decisions for BC depend on the grade, stage, and molecular subtype, which may include surgery, radiotherapy, and systemic therapies such as chemotherapy and targeted therapy. Radiotherapy plays a crucial role in preventing local recurrence of breast cancer and enhances the survival rate [4]. It is administered after breast-conserving surgery or mastectomy to target the tumor while protecting healthy surrounding tissues. Furthermore, advancements in radiotherapy techniques have raised the 15-year survival rate for early-stage BC to 80% [5-6]. This underscores the importance of minimizing doses to critical organs to reduce the risk of secondary cancers.

Treatment planning systems (TPS) are frequently utilized in clinics to calculate doses for target volumes and surrounding healthy tissues using various algorithms. However, TPSs have a significant limitation in determining doses in the out-of-field regions [7, 8]. Monte Carlo (MC) simulations are an emerging technique for accurately assessing radiation doses [7-12]. These simulations are employed to verify the accuracy of clinical treatment planning systems for dose calculations. Overall, the MC method provides greater accuracy for external photon or electron beam radiotherapy plans compared to treatment planning systems based on non-stochastic algorithms. Non-negligible differences have been reported in the results derived from both types of algorithms. Several studies have demonstrated that current commercial treatment planning systems tend to underestimate out-of-field doses [13, 14]. Out-of-field radiation includes scattering and leakage from the accelerator head, leading to inaccuracies in treatment planning systems [15, 16]. Furthermore, non-stochastic algorithms consistently generate inaccurate absorbed dose distributions in the presence of small radiation fields and areas with large mass density gradients, which starkly contrasts with general-purpose MC codes [17–21].

In recent years, the use of MC simulations for the

out-of-field region has increased [8, 9, 16, 22-25]. Assessing the doses received by healthy organs outside the treatment field is significantly important, as it directly impacts the probability of developing secondary cancer. In this context, several researchers have examined the radiation dose to a fetus of a pregnant mother who has undergone breast radiation therapy. The estimated radiation dose from the treatment planning system would not be accurate, as the fetus is located far from the radiation field [26-28].

In recent years, commercial treatment planning systems (TPSs) have been developed with tools that leverage fast MC-based algorithms [8]. Although their calculated dose is not as accurate as that of general-purpose MC codes, it still represents a significant advancement. However, due to their relatively high costs, these TPSs are not accessible in many clinics. On the other hand, there is a trend toward utilizing smaller and highly modulated radiation fields to enhance the tumor-to-normal tissue dose ratio [8]. This approach has spurred significant interest in MC treatment planning systems. As demand grows and research groups along with private companies show more interest in MC systems, additional resources will be allocated to developing self-contained systems focused on clinical applications. To achieve this goal, it will be crucial to significantly reduce the prolonged simulation times of general-purpose MC codes. The rise of affordable massive parallel computing is expected to have a major impact in this regard.

This study aims to validate the accuracy of MC modeling of a linear accelerator head for its application in 3D conformal radiotherapy (3DCRT) for breast cancer. This validation will involve comparing the MC results in the in-field region with those obtained from two different commercial Treatment Planning Systems (TPSs): Prowess Panther and RayStation. So far, no articles have focused on developing an MC tool for radiotherapy based on the MCNPX general-purpose code. Furthermore, the MC calculations in this study include three components: the upper part of the linear accelerator (linac), the lower part of the linac, and the computerized tomography (CT) representing the patient. This aspect serves as the unique element and novelty of this study. Additionally, the study aims to quantify the uncertainty in TPS dose calculations for out-of-field regions in the same treatment plan.

MATERIALS AND METHODS

In this study, a standard 3DCRT treatment plan was chosen for a patient with breast cancer. The treatment planning was conducted using the Prowess Panther Treatment Planning System version 5.50 (Panther, Prowess Inc., Chico, CA), and dose calculation was performed. The specifications for the six beams included in the treatment plan are shown in table 1 and figure 1. The treatment plan was imported into RayStation TPS (RaySearch Medical Laboratories AB, Stockholm, Sweden) for dose recalculation using its algorithm. The entire treatment plan was simulated using the MC method, and MC doses were evaluated and compared with the two TPSs.

Table 1. Beam characteristics of a typical 3D conformal radiation therapy (3DCRT) plan for a left breast cancer patient.

Name	Medial Beam	Lateral Beam	Supra-clavicular Beam	Posterior Beam	Medial Subfield	Posterior Subfield
Machine	AR-TISTE	AR-TISTE	ARTISTE	ARTISTE	ARTISTE	ARTISTE
Energy	6 MV *	6 MV *	6 MV *	6 MV *	6 MV *	6 MV *
Wedge Name	Open Field	Virtual Wedge	Open Field	Open Field	Open Field	Open Field
Wedge Orientation	-	Y1	-	-	-	-
Wedge Angle (°)	-	15.0	-	-	-	-
Collimator (°)	0.0	90.0	0.0	90.0	0.0	0.0
Field Size (cm)	19.2 × 21.5	21.0 × 19.0	17.8 × 6.0	5.5 × 17.5	7.8 × 11.5	11.9 × 6.0
Jaw 1 (cm)	X1:2.6 X2:16.6	X1:19.0 X2:2.0	X1:9.0 X2:8.8	X1:-2.0 X2:7.5	X1:2.8 X2:5.0	X1:5.7 X2:6.2
Jaw 2 (cm)	Y1:19.5 Y2:2.0	Y1:2.5 Y2:16.5	Y1:-2.0 Y2:8.0	Y1:9.0 Y2:8.5	Y1:9.0 Y2:2.5	Y1:3.0 Y2:3.0

* MV: Mega-Volt

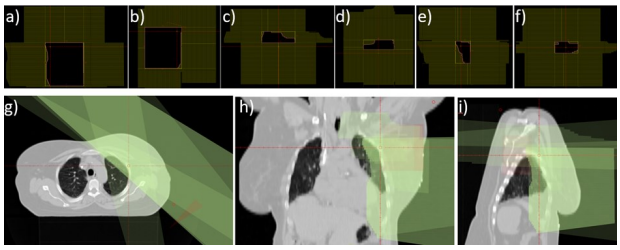


Figure 1. Beams' eye view of medial **(a)**, lateral **(b)**, supraclavicular **(c)**, posterior **(d)**, medial subfield **(e)**, and posterior subfield **(f)**, along with an axial **(g)**, coronal **(h)**, and sagittal **(i)** view of total beams on patient's planning CT images.

Developing the patient-specific phantom using CT images

The voxel model was created using planning CT images from a patient with left-sided breast cancer who had undergone a lumpectomy and was a candidate for 3DCRT. To create a voxel phantom that can be read by MC code, an in-house MATLAB code was utilized to extract the Hounsfield unit (HU) information from CT DICOM files. The HU values were then divided into seven ranges, as listed in table 2. Each range of HU was assigned an arbitrary non-repeating value representing the associated material composition and physical density. The voxel phantom was placed in the simulated geometry so that the isocenter point could be accurately positioned at (0 cm, 0 cm, and 100 cm).

A useful feature of the created phantom is its

ability to assess dose values within a specified structure. This is achieved by defining the organs according to radiation therapy (RT) structures that have been contoured and approved by the oncologist in the TPS. With this feature, we can calculate the mean doses impacting each OAR of interest. To address the issue, SlicerRT, an open-access 3D Slicer extension, was utilized to read the DICOM RT structure file [29]. Then, binary files related to each specified structure were extracted into files with the *.nrrd format. In the MC simulation, 15 distinct structures were assigned different identification numbers, referred to as universe numbers in the code. Additionally, heterogeneous materials were defined for each organ, and the organ density was determined based on the average HU values across the voxels included in the respective organ. Figure 2 illustrates the CT images and the voxel phantom, showcasing transverse, coronal, and sagittal views.

Table 2. The Hounsfield unit (HU) values and densities for various materials and tissues.

Materials and Tissues	HU values	Density (g/cm^3)
Air	-1024 to -942	0.001
Lung tissue	-942 to -212	0.385
Adipose tissue	-212 to -49	0.950
Soft tissue (Muscles)	-49 to 113	1.050
Spongy bone tissue	113 to 661	1.092
Compact bone tissue	661 to 1988	1.920
Enamel	1988 to 3070	2.750

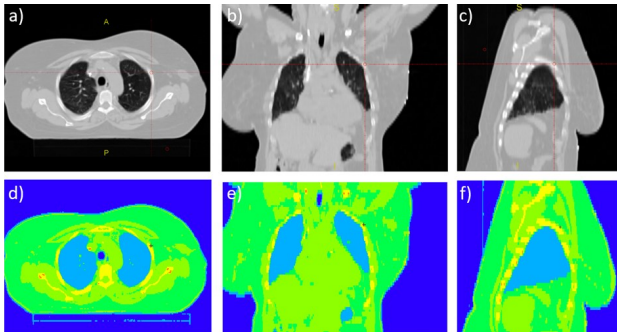


Figure 2. The CT image of selected patient in axial **(a)**, coronal **(b)**, and sagittal **(c)** views, together with voxel phantom created from CT images in the same views, respectively **(d-f)**.

Generating secondary PSFs for individual beams according to the treatment plan

Our research group has successfully modeled the linear accelerator (Linac) head and scored the information of particles exposed from a primary source and transported through the plan-independent part of the Linac head in a phase-space file (PSF). This information includes the position, direction, and energy of the particles (photons, electrons, and positrons). To ensure its accuracy, the primary PSF underwent benchmarking by comparing results with Linac commissioning data, as described in Tuğrul *et al.* [30]. Using models of jaws and MLC, the primary PSF was utilized to generate secondary PSFs located just below the MLC. For a clearer understanding of the process, please refer to figure 3. The MC simulation was done by MC N-particle Transport Code Extended (MCNPX version 2.6.0, Los Alamos, USA).

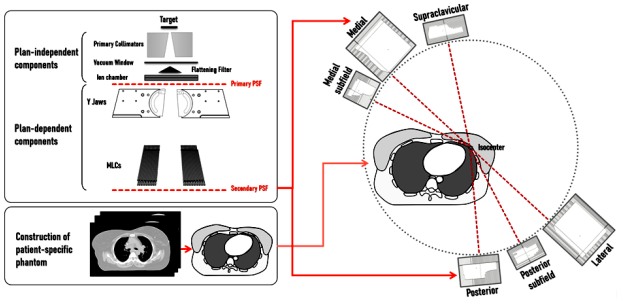


Figure 3. Process of Monte Carlo simulation of a typical treatment plan used in this study was displayed in this figure.

Applying treatment beams to the patient-specific phantom

According to the treatment plan, secondary PSFs were generated for six beams of the typical plan, which include medial, lateral, supraclavicular, posterior, and two subfields, as shown in figure 4. The secondary PSFs were utilized to virtually expose the computational patient-specific phantom in the direction of the respective beam figure 4.

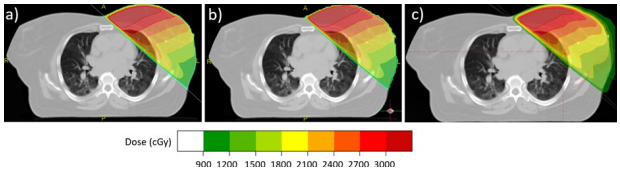


Figure 4. Dose distributions for the medial beam from Prowess Panther **(a)**, RayStation **(b)** and Monte Carlo **(c)**.

Dose calculation: in-field and out-of-field

In-field: The energy deposition per volume in the in-field region was estimated using the mesh tally feature of the MCNPX code based on the MC dose distribution. To achieve this, a type 3 mesh tally was implemented to score the energy deposition per unit volume in MeV/cm^3. After dividing these values by the physical density of each voxel, they were converted into MeV/g. Finally, the values were transformed into Gray using equation (1).

$$Dose_{Beam}\,(cGy) = Tally_{Beam}\left(\frac{MeV}{g}\right) \times 160.218 \times 10^{10}\left(\frac{\frac{cGy}{MeV}}{g}\right) \times C\left(\frac{particles}{MU}\right) \times N_{Beam}(MU) \qquad (1)$$

Where: Tally represents the output of the MC code in MeV/g, 160.218×10^{10} is a constant coefficient that converts MeV/g to cGy, C is the normalization coefficient determining the number of particles associated with 1 Monitor Unit (MU), and N denotes the number of MUs associated with each individual beam.

Out-of-field: To determine the mean doses received by OARs located near the edge of the radiation field or outside of it, the energy deposition per organ mass was scored using the +F6 tallies. A total of 8×10^{11} particle histories was simulated, resulting in statistical errors of less than 0.6%. This indicates that

the MC dose estimation is sufficiently reliable.

Comparative analysis

Dose distributions obtained from the Monte Carlo (MC) simulations and the two commercial treatment planning systems (TPSs) were compared in three dimensions using gamma index analysis. The global gamma evaluation method was applied with acceptance criteria of 3%/3 mm and a dose threshold of 10%. Additionally, isodose curves were visually compared on selected 2D slices to assess spatial agreement. Dose-volume histograms (DVHs) were generated and analyzed for the clinical target volume (CTV), target nodal regions, and organs at risk (OARs), including the ipsilateral lung, left anterior descending (LAD) artery, and heart. A two-tailed t-test was performed to statistically assess the differences in calculated dose metrics between methods, with p-values computed to determine the significance of observed variations.

RESULTS

Monte Carlo (MC) simulations were performed for a standard 3DCRT plan for a breast cancer patient, and the results were compared with dose calculations from two treatment planning systems (TPSs), Prowess Panther and RayStation. The findings are presented in two subsections: in-field and out-of-field regions, with quantitative comparisons, including statistical significance (p-values) where applicable.

In-field region

A comprehensive analysis of dose distributions was conducted using isodose maps, dose-volume histograms (DVHs), and dose profiles. Figure 4 illustrates the dose distribution for the medial beam, calculated by three distinct systems: Prowess Panther (a), RayStation (b), and Monte Carlo simulation (c). In all three panels, a computed tomography (CT) scan of the thoracic region is superimposed, and the dose map is color-coded from green (lower dose) to dark red (higher dose). A comparative analysis demonstrates that our Monte Carlo modeling results in dose distributions within the treatment field that closely resemble those generated by commercial treatment planning systems. This visual concordance of isodose curves within the field corroborates the reliability and consistency of our simulation in this region. Figure 5 presents Monte Carlo-based isodose distributions across four distinct axial slices (a–d). These slices were selected to encompass varying anatomical regions, facilitating a comprehensive evaluation of relative dose uniformity within the target volume, as previously planned.

To quantify this agreement, gamma index analysis (3%/3 mm, global normalization, 10% threshold) was performed. As shown in table 3, the gamma passing rates (GPRs) for individual beams ranged from 94.3% to 99.2% (MC vs. Prowess Panther, $p<0.001$) and from 96.0% to 99.0% (MC vs. RayStation, $p<0.001$). For composite beams, GPRs were 91.2% (MC vs. Prowess Panther, $p<0.001$) and 94.3% (MC vs. RayStation, $p<0.001$). Statistical analysis (two-tailed t-test) confirmed that while the GPRs indicate a high degree of conformity between the two datasets, they remain statistically distinct ($p<0.001$ for all comparisons).

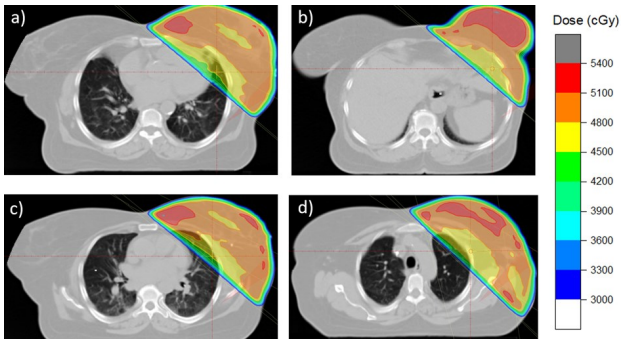


Figure 5. Monte Carlo dose distributions in four different slices.

Table 3. The global gamma passing rates (GPRs) for individual beams and total beams with criteria of 3%/3mm and 10% dose threshold.

Beams	Global gamma passing rate (%) *	
	Monte Carlo vs. TPS (Prowess Panther 5.50)	Monte Carlo vs. TPS (RayStation)
Medial	95.94	96.09
Lateral	94.33	98.18
Posterior	98.69	99.00
Supraclavicular	99.18	96.02
Medial subfield	98.97	98.93
Posterior subfield	97.77	98.59
Total Beams	91.21	94.25

* For all comparisons, the p-value was less than 0.001.
** TPS: Treatment Planning System.

Figure 6 displays the dose-volume histogram (DVH) curves for clinical target volumes (CTVs), regional lymph nodes (supraclavicular and axillary), and organs at risk (OARs: heart, left anterior descending artery [LAD], and left lung). While the Monte Carlo (MC) and treatment planning system (TPS)-derived DVHs showed close alignment, minor discrepancies were observed in both target and OAR regions. Nevertheless, the overall agreement suggests that the MC model demonstrates reasonably good consistency with commercial TPS algorithms.

Figure 7 compares the dose profiles (lateral, medial, and composite beams) along a representative dashed line, presenting data from MC (dashed line), Prowess (solid line), and RayStation (dotted line). The discrepancies were most evident in the lateral beam, while the medial beam displayed relatively acceptable agreement. This divergence likely arises from inherent limitations in TPS modeling, particularly as the lateral beam traverses a significant portion of treatment devices, such as the couch.

Out-of-field region

In the area beyond the treatment field, the results are presented as the mean doses received by the OARs. The table outlines the mean doses for 15 organs located at or near the edge of a field or in the out-of-field region. Out-of-field doses to OARs were systematically underestimated by both TPSs (table 4). Prowess Panther underestimated doses by as much as 47% (mean: 23.5 ± 10.2%, p<0.001), while RayStation exhibited larger deviations (up to 94%, mean: 32.1 ± 22.3%, p<0.001). The most significant discrepancies occurred in low-density tissues (e.g., right kidney: −93.8% for RayStation).

Figure 8 illustrates the percentage dose differences (TPS vs. MC) fitted to exponential decay functions (R^2 = 0.95–0.98). Masked data (gray symbols) were excluded from the fitting process. The trends emphasize the limitations of TPS in predicting peripheral scatter, especially beyond 5 cm from the edges of the field (p < 0.001 for distance-dependent bias).

Table 4. Mean absorbed doses for 15 organs and dose differences between Treatment Planning Systems (TPSs) versus Monte Carlo.

Organ name	Mean Dose (cGy)			Dose difference (%)*	
	Prowess Panther	RayStation	Monte Carlo	Prowess Panther vs. Monte Carlo	RayStation vs. Monte Carlo
Right Breast (contralateral)	47.8	46.2	72.4 (0.1%)	-33.95	-36.16
Esophagus	91.4	70.4	108.1 (0.3%)	-15.42	-34.85
Trachea	892.5	939.3	1237.1 (0.2%)	-27.86	-24.07
Thyroid	2248.8	2269.1	2292.6 (0.2%)	-1.91	-1.02
Left Kidney	50.2	39.7	64.3 (0.2%)	-21.96	-38.28
Right Kidney	16.7	1.6	26.0 (0.6%)	-35.71	-93.84
Liver	51.9	35.4	67.7 (0.1%)	-23.34	-47.71
Right Lung (contralateral)	66.5	51.6	81.8 (0.1%)	-18.68	-36.90
Pancreas	61.4	54.5	80.0 (0.2%)	-23.23	-31.86
Spinal Cord	190.8	184.8	301.1 (0.2%)	-36.63	-38.62
Spleen	112.7	111.3	141.7 (0.1%)	-20.47	-21.46
Stomach	119.5	194.9	223.9 (0.1%)	-46.63	-12.96
Heart	655.5	626.2	656.2 (0.0%)	-0.11	-4.57
LAD	4350.4	4231.8	4269.6 (0.2%)	1.89	-0.89
Left lung	1475.8	1421.1	1474.2 (0.0%)	0.11	-3.60

*For all dose differences, the p-value was less than 0.001, indicating a statistically significant difference.

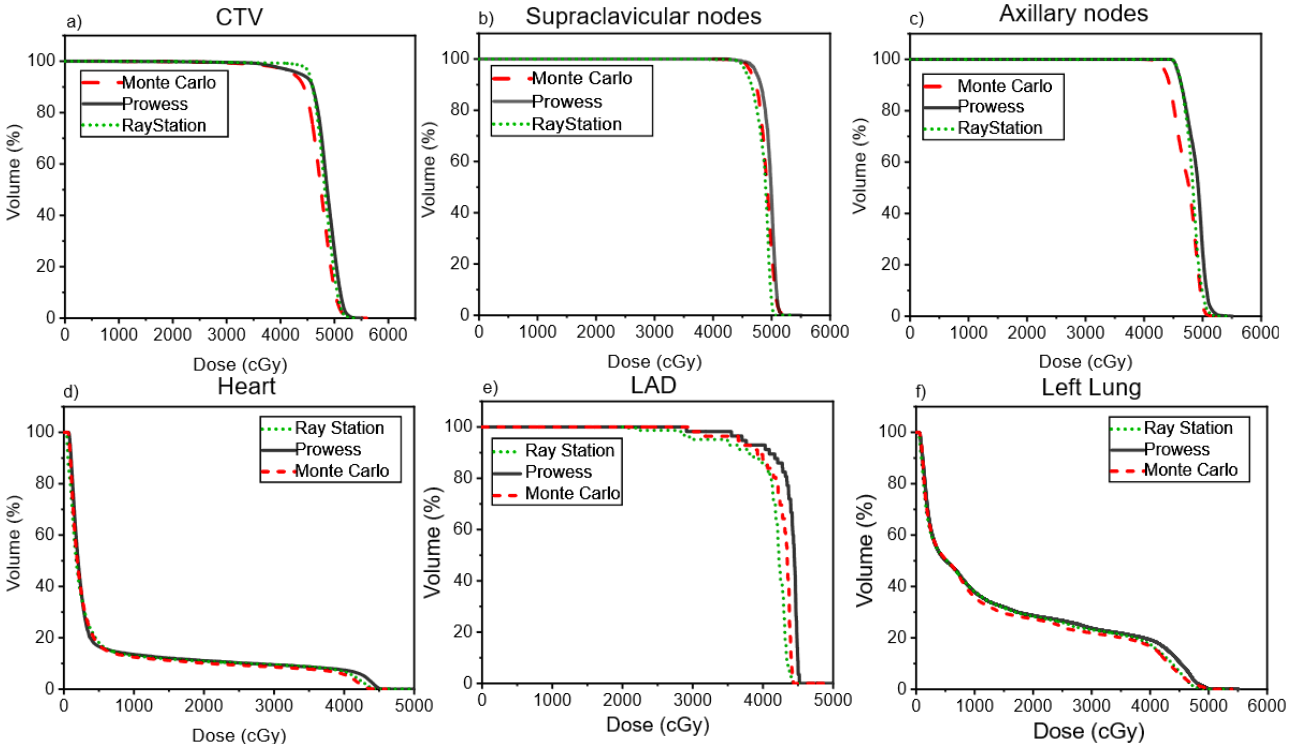


Figure 6. DVH curves for **(a)** CTV, **(b)** supraclavicular nodes, **(c)** axillary nodes, and **(d)** OARs including heart, **(e)** LAD, and **(f)** left lung.

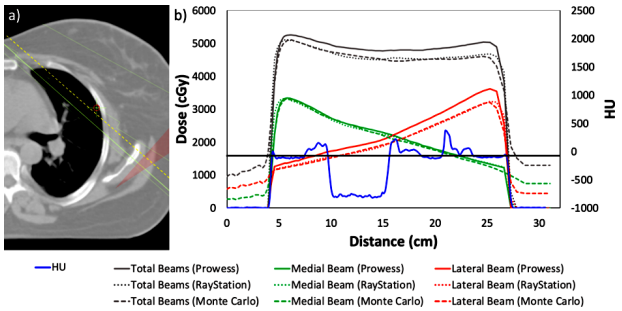


Figure 7. (a) Location of the dose profile line superimposed on the patient's CT image. **(b)** HU values along the same line comparing Monte Carlo, and Treatment Planning System calculations (Prowess Panther 5.50, and RayStation).

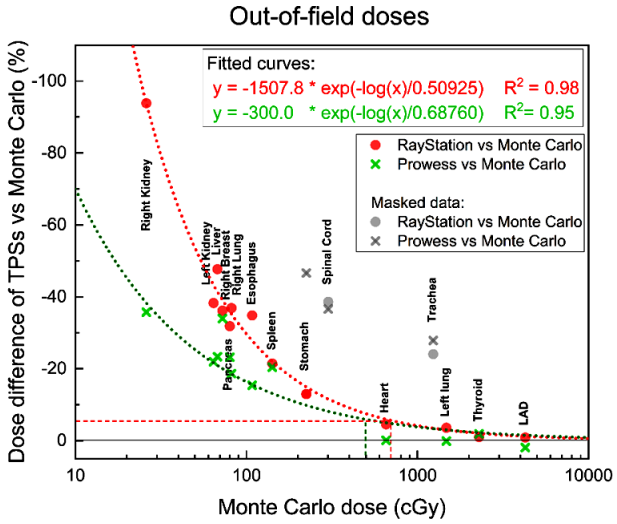


Figure 8. The percentage differences in out-of-field doses were calculated by TPSs versus Monte Carlo doses. The red circle symbol is used for RayStation data, and the green cross-line symbol is used for Prowess. The red and green lines were fitted to RayStation and Prowess data, respectively. Gray symbols were masked data.

DISCUSSION

Monte Carlo (MC) simulation codes such as Geant4, EGSnrc, and MCNP have become essential in medical physics, particularly for radiotherapy dose calculations where they serve as the gold standard [31]. Their advantage lies in their ability to model radiation transport accurately through heterogeneous media, especially in challenging situations involving small fields or tissue interfaces [32]. Our study utilized MCNPX, acknowledging its superior accuracy, despite the fact that it's 50 to 100 times slower than faster MC codes like EGSnrc.

Recent advancements by Witte *et al.* show how deep learning can accelerate MC calculations by 82× while maintaining 99.6% gamma passing rates (2%/2mm), indicating promising routes to mitigate the computational burden [33]. Likewise, Franciosini *et al.* achieved 200 to 5000× speed improvements through GPU acceleration in their FRED software while preserving 2% accuracy [31]. These advancements tackle the main limitation of MC methods - their computational intensity - while upholding their unmatched accuracy.

Our findings align with several recent studies comparing MC to commercial TPS in-field doses. Similar to Lin *et al.* [34], who found 2-5% differences between EGS4/MCSIM and Eclipse AAA for SBRT plans, we observed that RayStation showed better agreement with MC than Prowess Panther, particularly for CTV (2.2% difference) and ipsilateral lung (4% difference). The gamma passing rates for individual beams exceeded those for composite plans, akin to the findings by Goodall *et al.* in their Monaco TPS study [35]. Notably, Cheng *et al.* demonstrated how algorithm choice affects accuracy near heterogeneities, with AAA showing 15-25% overestimations behind metal implants compared to DOSXYZnrc MC [36]. Our DVH analysis similarly revealed a consistent overestimation trend with Prowess Panther, emphasizing that different TPS algorithms require careful validation against MC benchmarks, especially in complex geometries.

Our most striking findings concern out-of-field doses, where both TPS underestimated doses by 47-94%, particularly for organs such as the right kidney. This aligns perfectly with Meyer *et al.* using TOPAS, who emphasized MC's critical role in out-of-field risk assessment [37]. The exponential increase in TPS underestimation with distance from the field edge matches observations by Livingstone *et al.* in their EGSnrc validation of VMAT plans [38]. The spinal cord and trachea dose anomalies in our data, which deviate from the exponential trend, likely result from partial volume effects near field edges, mirroring findings reported by Zhang *et al.* in their CNN-based dose prediction study [39]. Our results confirm that current TPS algorithms remain inadequate for out-of-field dose prediction, leading to potentially dangerous underestimates of secondary cancer risks.

Our study contributes to the growing evidence that MC methods should become standard for both treatment planning and verification. While commercial TPS like RayStation perform reasonably well in-field (particularly with advanced algorithms like AcurosXB), their out-of-field inaccuracies remain clinically significant. The development of fast MC implementations suggests that clinical adoption is becoming feasible [31, 33]. Future work should focus on: (1) Implementing AI-accelerated MC engines like T-MC Net for routine clinical use [40], and (2) Establishing MC-based out-of-field dose constraints for secondary cancer prevention. Our validation of this MC model creates a foundation for developing an in-house QA tool that could significantly improve 3DCRT plan accuracy, particularly for out-of-field dose assessment where current TPS fail dramatically. Furthermore, we aim to develop a validated Monte Carlo model that will subsequently (1) be integrated into fast Monte Carlo-based treatment planning systems and (2) provide benchmark data for

developing and training AI-driven dose calculation algorithms.

CONCLUSION

This study validated the Monte Carlo (MC) model for the Artiste Siemens linear accelerator in 3D conformal radiation therapy (3DCRT) for breast cancer. Among the evaluated treatment planning systems (TPSs), RayStation showed greater accuracy in calculating in-field doses, closely aligning with MC results. However, both TPSs had significant limitations in estimating out-of-field doses for organs receiving less than 500–700 cGy, raising concerns about secondary cancer risks. While commercial TPS algorithms perform adequately within the treatment field, our findings underscore that MC simulations remain the gold standard for dose calculations, particularly in out-of-field regions.

Funding: The research of the corresponding author is supported by a grant from Ferdowsi University of Mashhad (N.3/50392).

Disclosures: None.

Author contribution statements: H.M. devised the project, including the main conceptual ideas and the proof outline. N.R. and E.H. developed nearly all the technical details and conducted the Monte Carlo calculations. T.T. executed treatment planning using the RayStation treatment planning system. M.D., as a radiation oncologist, delineated the target and organs at risk (OAR) for the breast cancer patient and assessed the clinical aspects of treatment planning. E.H. and H.M. composed the manuscript. H.M. supervised the project.

Conflicts of interest statement: The authors certify that they have no affiliations with, or involvement in, any organization or entity that holds any financial or non-financial interest in the subject matter or materials discussed in this manuscript.

REFERENCES

1. Lima SM, Kehm RD, Terry MB (2021) Global breast cancer incidence and mortality trends by region, age-groups, and fertility patterns. *EClinical Medicine*, ***1**: 38*.
2. Sung H, Ferlay J, Siegel RL, Laversanne M, *et al.* (2021) Global cancer statistics 2020: GLOBOCAN estimates of incidence and mortality worldwide for 36 cancers in 185 countries. *CA: A Cancer journal for Clinicians*, ***71**(3):209-49.*
3. Rossi L, Mazzara C, Pagani O (2019) Diagnosis and treatment of breast cancer in young women. *Current Treatment Options in Oncology*, ***20**(12): 86.*
4. Bronsart E, Dureau S, Xu HP, Bazire L, Chilles A, *et al.* (2017) Whole breast radiotherapy in the lateral isocentric lateral decubitus position: Long-term efficacy and toxicity results. *Radiotherapy and Oncology*, ***124**(2): 214-9.*
5. da Luz FA, da Costa Marinho E, Nascimento CP, de Andrade Marques L, *et al.* (2022) The effectiveness of radiotherapy in preventing disease recurrence after breast cancer surgery. *Surgical Oncology*, ***41**: 101709.*
6. Yoshimura A, Ito H, Nishino Y, Hattori M, *et al.* (2018) Recent improvement in the long-term survival of breast cancer patients by age and stage in Japan. *Journal of Epidemiology*, ***28**(10): 420-7.*
7. Guatelli S and Incerti S (2017) Monte Carlo simulations for medical physics: From fundamental physics to cancer treatment. *Physica Medica: European Journal of Medical Physics*, ***33***: *179-81*.
8. Brualla L, Rodriguez M, Lallena AM (2017) Monte Carlo systems used for treatment planning and dose verification. *Strahlentherapie und Onkologie, **193**(4)*: *243*.
9. Liang Y, Muhammad W, Hart GR, Nartowt BJ, *et al.* (2020) A general-purpose Monte Carlo particle transport code based on inverse transform sampling for radiotherapy dose calculation. *Scientific Reports, **10**(1): 9808*.
10. Berris T, Mazonakis M, Stratakis J, Tzedakis A, *et al.* (2013) Calculation of organ doses from breast cancer radiotherapy: a Monte Carlo study. *Journal of Applied Clinical Medical Physics, **14** (1)*: *133-46*.
11. Kairn T, Livingstone AG, Crowe SB (2020) Monte Carlo calculations of radiotherapy dose in "homogeneous" anatomy. *Physica Medica*, ***78**: 156-65*.
12. Arce P, Lagares JI, Azcona JD, Huesa-Berral C, Burguete J (2023) Precise dosimetric comparison between GAMOS and the collapsed cone convolution algorithm of 4D DOSE accumulated in lung SBRT treatments. *Radiation Physics and Chemistry*, ***208**: 110891*.
13. Brualla L, Palanco-Zamora R, Wittig A, *et al.* (2009) Comparison between PENELOPE and electron Monte Carlo simulations of electron fields used in the treatment of conjunctival lymphoma. *Physics in Medicine and Biology, **54***: *5469-5481*.
14. Panettieri V, Barsoum P, Westermark M, *et al.* (2009) AAA and PBC calculation accuracy in the surface build-up region in tangential beam treatments. Phantom and breast case study with the Monte Carlo code PENELOPE. *Radiotherapy and Oncology, **93**: 94 -101*.
15. Huang JY, Followill DS, Wang XA, Kry SF (2013) Accuracy and sources of error of out of field dose calculations by a commercial treatment planning system for intensity-modulated radiation therapy treatments. *J Appl Clin Med Phys, **14**(2)*: 186-97
16. Sánchez-Nieto B, Medina-Ascanio KN, Rodríguez-Mongua JL, *et al.* (2020) Study of out-of-field dose in photon radiotherapy: A commercial treatment planning system versus measurements and Monte Carlo simulations. *Medical Physics, **47**(9): 4616-25*.
17. Das IJ, Ding GX, Ahnesjö A (2008) Small fields: nonequilibrium radiation dosimetry. *Medical physics*, ***35***: *206–215*.
18. Brualla L, Palanco-Zamora R, Steuhl K-P, *et al.* (2011) Monte Carlo simulations applied to conjunctival lymphoma radiotherapy treatment. *Strahlentherapie und Onkologie*, ***187**: 492-498*.
19. Brualla L, Mayorga PA, Flühs A, *et al.* (2012) Retinoblastoma external beam photon irradiation with a special "D"-shaped collimator: a comparison between measurements, Monte Carlo simulation and a treatment planning system calculation. *Physics in Medicine and Biology, **57**: 7741-7751*.
20. Brualla L, Zaragoza FJ, Sempau J, *et al.* (2012) Electron irradiation of conjunctival lymphoma-Monte Carlo simulation of the minute dose distribution and technique optimization. *Int J Radiat Oncol Biol Phys*, ***83**:1330–1337*.
21. Mayorga PA, Brualla L, Sauerwein W, *et al.* (2014) Monte Carlo study for designing a dedicated "D"-shaped collimator used in the external beam radiotherapy of retinoblastoma patients. *Medical physics, **41**: 011714*.
22. Takata T, Shiraishi K, Kumagai S, Arai N, *et al.* (2020) Calculating and estimating second cancer risk from breast radiotherapy using Monte Carlo code with internal body scatter for each out-of-field organ. *J Appl Clin Med Phys, **21**(12): 62-73*.
23. De Saint-Hubert M, Suesselbeck F, Vasi F, Stuckmann F, *et al.* (2022) Experimental validation of an analytical program and a Monte Carlo simulation for the computation of the far out-of-field dose in external beam photon therapy applied to pediatric patients. *Frontiers in Oncology, **7**(12): 882506*.
24. Al-Saleh WM and Hugtenburg RP (2023) Monte Carlo modelling of a 6 MV Elekta linear accelerator for in-field and out-of-field dosimetry. *Radiation Physics and Chemistry*, ***203**:110584*.
25. Ghareeb F, Esposito A, Lencart J, Santos JA (2020) Localized extra focal dose collimator angle dependence during VMAT: An out-of-field Monte Carlo study using PRIMO software. *Radiation Physics and Chemistry*, ***171**:108694*.
26. Sushma N, Kaginelli S, Sathiyaraj P, Manikandan PS, Ganesh KM (2023) Analysis of fetal dose using Optically Simulated Luminescence Dosimeter and ion chamber in randophantom for various radiotherapy techniques. *Applied Radiation and Isotopes*, ***198***:110854.
27. Mazonakis M and Damilakis J (2017) Estimation and reduction of the radiation dose to the fetus from external-beam radiotherapy.

Physica Medica, ***43****:148-52*.
28. Mazonakis M, Tzedakis A, Damilakis J (2017) Monte Carlo simulation of radiotherapy for breast cancer in pregnant patients: how to reduce the radiation dose and risks to fetus? *Radiation Protection Dosimetry*. ***175****(1)*:10-6.
29. Pinter C, Lasso A, Wang A, Jaffray D, Fichtinger G (2012) SlicerRT: radiation therapy research toolkit for 3D Slicer. *Medical Physics,* ***39****: 6332-6337*.
30. Tuğrul T and Eroğul O (2019) Determination of initial electron parameters by means of Monte Carlo simulations for the Siemens Artiste Linac 6MV photon beam. *Reports of Practical Oncology and Radiotherapy,* ***24****(4): 331-7*.
31. Franciosini G, Battistoni G, Cerqua A, De Gregorio A, *et al.* (2023) GPU-accelerated Monte Carlo simulation of electron and photon interactions for radiotherapy applications. *Physics in Medicine & Biology,* ***68****(4): 044001*.
32. Kumar S, Nahum AE, Chetty IJ (2020). Monte-Carlo-computed dose, kerma and fluence distributions in heterogeneous slab geometries irradiated by small megavoltage photon fields. *Physics in Medicine & Biology*, ***65****(17): 175012*.
33. Witte M and Sonke JJ (2024) A deep learning based dynamic arc radiotherapy photon dose engine trained on Monte Carlo dose distributions. *Physics and Imaging in Radiation Oncology,* ***30****: 100575*.
34. Lin T, Wang L, Charlie CM (2022) Monte Carlo dose calculation–a QA method for SRT and SBRT plans in treating multiple and small metastatic lesions. *Journal of Medical Physics,* ***47****(1): 99-104*.
35. Goodall SK and Ebert MA (2020) Recommended dose voxel size and statistical uncertainty parameters for precision of Monte Carlo dose calculation in stereotactic radiotherapy. *Journal of Applied Clinical Medical Physics,* ***21****(12): 120-130*.
36. Cheng ZJ, Bromley RM, Oborn B, Booth JT (2021) Radiotherapy dose calculations in high-Z materials: comprehensive comparison between experiment, Monte Carlo, and conventional planning algorithms. *Biomedical Physics & Engineering Express,* ***7****(3): 035012*.
37. Meyer I, Peters N, Tamborino G, Lee H, *et al.* (2024) A framework for in-field and out-of-field patient specific secondary cancer risk estimates from treatment plans using the TOPAS Monte Carlo system. *Physics in Medicine & Biology,* ***69****(16): 165023*.
38. Livingstone AG, Crowe SB, Sylvander S, Kairn T (2020) Clinical implementation of a Monte Carlo based independent TPS dose checking system. *Physical and Engineering Sciences in Medicine,* ***43*** *(3): 1113-1123*.
39. Zhang B, Liu X, Chen L, Zhu J (2022) Convolution neural network toward Monte Carlo photon dose calculation in radiation therapy. *Medical Physics,* ***49****(2): 1248-1261*.
40. Colson D, Blommaert J, Poels K, De Saint-Hubert M, *et al.* (2023) Extended in-field and out-of-field validation of a compact Monte Carlo model of an IBA PROTEUS® ONE proton beam in TOPAS/GEANT4. *Physics in Medicine & Biology*, ***68****(21): 21NT02*.